International Journal of Pharmaceutics 434 (2012) 80–89

Contents lists available at SciVerse ScienceDirect

International Journal of Pharmaceutics

journal homepage: www.elsevier.com/locate/ijpharm

Influence of skin model on *in vitro* performance of drug-loaded soluble microneedle arrays

Martin J. Garland[a], Katarzyna Migalska[a], Tuan-Mazlelaa Tuan-Mahmood[b], Thakur Raghu Raj Singh[a], Rita Majithija[a], Ester Caffarel-Salvador[a], Cian M. McCrudden[a], Helen O. McCarthy[a], A. David Woolfson[a], Ryan F. Donnelly[a,*]

[a] *School of Pharmacy, Queen's University Belfast, Medical Biology Centre, 97 Lisburn Road, Belfast BT9 7BL, UK*
[b] *Faculty of Pharmacy, The National University of Malaysia (UKM), Jalan Raja Muda Abdul Aziz, 50300 Kuala Lumpur, Malaysia*

ARTICLE INFO

Article history:
Received 20 March 2012
Accepted 25 May 2012
Available online 2 June 2012

Keywords:
Microneedles
Transdermal drug delivery
Skin model
In vitro release

ABSTRACT

A plethora of studies have described the *in vitro* assessment of dissolving microneedle (MN) arrays for enhanced transdermal drug delivery, utilising a wide variety of model membranes as a representation of the skin barrier. However, to date, no discussion has taken place with regard to the choice of model skin membrane and the impact this may have on the evaluation of MN performance. In this study, we have, for the first time, critically assessed the most common types of *in vitro* skin permeation models – a synthetic hydrophobic membrane (Silescol® of 75 μm) and neonatal porcine skin of definable thickness (300–350 μm and 700–750 μm) – for evaluating the performance of drug loaded dissolving poly (methyl vinyl ether co maleic acid) (PMVE/MA) MN arrays. It was found that the choice of *in vitro* skin model had a significant effect on the permeation of a wide range of small hydrophilic molecules released from dissolving MNs. For example, when Silescol® was used as the model membrane, the cumulative percentage permeation of methylene blue 24 h after the application of dissolvable MNs was found to be only approximately 3.7% of the total methylene blue loaded into the MN device. In comparison, when dermatomed and full thickness neonatal porcine skin were used as a skin model, approximately 67.4% and 47.5% of methylene blue loaded into the MN device was delivered across the skin 24 h after the application of MN arrays, respectively. The application of methylene blue loaded MN arrays in a rat model *in vivo* revealed that the extent of MN-mediated percutaneous delivery achieved was most similar to that predicted from the *in vitro* investigations employing dermatomed neonatal porcine skin (300–350 μm) as the model skin membrane. On the basis of these results, a wider discussion within the MN community will be necessary to standardise the experimental protocols used for the evaluation and comparison of MN devices.

1. Introduction

The transdermal route allows for surmounting obstacles associated with oral and parenteral administration of drugs and provides a convenient and patient-friendly means of delivering therapeutics (Banga, 2006; Gupta and Sharma, 2009). However, the main limitation of transdermal drug delivery is skin's limited permeability, due to its outermost layer, the *stratum corneum* (*SC*), which significantly restricts the spectrum of drugs that can efficiently traverse the skin. To date, numerous methods aiming at increasing transdermal drug transport have been evaluated, including: chemical penetration enhancers (Karande et al., 2004), microneedles (MNs) (Fukushima et al., 2010), ultrasound (Park et al., 2007), iontophoresis (Medi and Singh, 2003), electroporation (Tokumoto et al., 2006), thermal (Badkar et al., 2007), laser (Fujiwara et al., 2005) and radiofrequency (Sintov et al., 2003) poration. Among these techniques, MNs stand out as a simple and relatively low cost approach of high promise.

MN devices are composed of micron-size needles which have the ability to physically disrupt the *SC* and create aqueous microconduits for hydrophilic drugs to pass through the deeper layers of the skin to the microcapillary bed for systemic absorption (Prausnitz, 2004). MN technology has been demonstrated to be painless (Kaushik et al., 2001) and blood-free (Bal et al., 2008; Van Damme et al., 2009). MNs have been fabricated in a wide range of designs from various materials, including silicon (Wilke et al., 2005), glass (McAllister et al., 2003), metal (Cormier et al., 2004) and polymers (Sullivan et al., 2008, 2010; Chu et al., 2010). MNs have been shown to improve transdermal delivery of a wide range of hydrophilic molecules (Fukushima et al., 2010; McAllister et al., 2003; Cormier et al., 2004; Sullivan et al., 2008; Chu et al., 2010; Henry et al., 1998; Gardeniers et al., 2003; Kolli and Banga, 2008; Jiang et al., 2009; Park et al., 2005; Ito et al., 2006; Ameri et al.,

* Corresponding author. Tel.: +44 028 9097 2251; fax: +44 028 9024 7794.
E-mail address: r.donnelly@qub.ac.uk (R.F. Donnelly).

0378-5173/$ – see front matter © 2012 Elsevier B.V. All rights reserved.
http://dx.doi.org/10.1016/j.ijpharm.2012.05.069

2010; Matriano et al., 2002; Widera et al., 2006; Martanto et al., 2004; Roxhed et al., 2008).

A variety of different approaches have been utilised to investigate MN-mediated percutaneous drug transport. To study the release of calcein encapsulated within PLGA MNs, MN arrays were inserted into full-thickness human cadaver skin and, after MN removal, confocal microscopy was employed to study the spatial distribution of calcein (Park et al., 2006). Sullivan et al. (2008) used fluorescence microscopy to study the distribution of Texas Red-labelled bovine serum albumin in porcine skin following release from poly(vinylpyrolidone) MNs.

To quantify *in vitro* drug release from polymeric MNs, a set-up consisting of 30-ml glass vials filled with receptor medium, magnetically stirred and incubated at 37 °C has been employed (Park et al., 2006). However, Franz cells, a well-established system for *in vitro* testing of pharmaceutical semi-solid dosage forms for transdermal applications, are most commonly employed to assess MN-mediated transdermal drug delivery *in vitro*. A range of skin models, including synthetic membranes, heat separated epidermis, dermatomed and full-thickness skin (Coulman et al., 2009; Lee et al., 2008; Verbaan et al., 2007; Li et al., 2009) have all been used. Whilst a variety of texts have outlined the choice of these membranes as a representation of the skin barrier for the evaluation of conventional patch- or gel-based transdermal dosage forms (Williams, 2003; Banga, 2011), to date, there has been no general consensus, or discussion, on the choice of skin model for the *in vitro* evaluation of MN-mediated transdermal drug delivery.

The purpose of the present study was to, for the first time, investigate the effect of skin model choice on MN-mediated *in vitro* percutaneous delivery of a variety of small molecular weight hydrophilic compounds released from dissolving polymeric MN arrays.

2. Materials and methods

2.1. Chemicals

Gantrez® AN-139, a copolymer of methylvinylether and maleic anhydride (PMVE/MAH) was provided by ISP Co. 120 Ltd., Guildford, UK. Theophylline, caffeine anhydrous, lidocaine HCl, methylene blue, fluorescein sodium, and metronidazole were obtained from Sigma–Aldrich, Dorset, UK. Silescol® 7-4107 silicone membrane was a gift from Dow Corning Europe S.A. (Seneffe, Belgium). All other chemicals used were of analytical reagent grade.

2.2. Fabrication of drug-loaded MNs prepared from aqueous blends of 20% w/w PMVE/MA

MNs prepared from aqueous blends of 20% w/w poly (methyl vinyl ether co maleic acid) (PMVE/MA) and loaded with model drugs were prepared using laser-engineered silicone micromould templates, as described previously (Donnelly et al., 2011; Migalska et al., 2011). Briefly, silicone elastomer was poured into a custom-made aluminium mould and cured overnight at 40 °C. A laser-machine tool (BluLase® Micromachining System, Blueacre Technology, Dundalk, Ireland) with a laser (Coherent Avia, Coherent Inc., Pittsburgh, USA) emitting a beam having a wavelength of 355 nm and a pulse length of 30 ns (variable from 1 to 100 kHz) was then employed to produce MN moulds (11 × 11 array, 600 μm height, 300 μm width and 300 μm interspacing at MN base). A 30% w/w aqueous solution of PMVE/MA was prepared by adding the required mass of PMVE/MAH to ice-cold deionised water, followed by vigorous stirring and heating at 95.0 °C until a clear gel was obtained, due to hydrolysis of the anhydride form of the copolymer to the corresponding acid. Upon cooling, the blend was then readjusted to the final concentration of 30% w/w by the addition of an appropriate amount of deionised water. To prepare drug-loaded MNs, the stock solution was diluted with the appropriate amount of water, in which the amount of model drugs necessary to obtain desired loadings per MN device (Table 1) (whereby 3.10 mg caffeine, 7.26 mg lidocaine, 3.5 mg fluorescein sodium, 3.5 mg methylene blue, 4.80 mg metronidazole, 3.5 mg theophylline were distributed throughout the entire MN array, *i.e.* within the MNs and MN base plate, for each case) was dissolved, to obtain MNs composed of 20% w/w PMVE/MA gel. An aliquot of 0.5 g of the obtained solution was then poured into the silicone micromould, centrifuged for 15.0 min at 3500 rpm and allowed to dry under ambient conditions for 24 h (Donnelly et al., 2011). Control patches were prepared by pouring a 0.5 g aliquot of the drug loaded PMVE/MA gel into silicone micromoulds, containing no laser engineered MN holes, which were then allowed to dry under ambient conditions for 24 h (Donnelly et al., 2011).

2.3. In vitro drug permeation studies using Franz cells

Diffusion of model drugs from polymeric MN arrays across the model silicone membrane, Silescol® (75 μm thick), dermatomed (300–350 μm thick) and full-thickness (700–750 μm thick) neonatal porcine skin was investigated *in vitro* using modified Franz diffusion cells (FDC-400 flat flange, 15 mm orifice diameter, mounted on an FDCD diffusion drive console providing synchronous stirring at 600 rpm and thermostated at 32 ± 1 °C) (Crown Glass Co. Inc., Sommerville, NJ, USA). Receptor compartment volumes, approximately 12 ml, were exactly determined by triplicate measurements of the weights of water they could accommodate. Skin samples were obtained from stillborn piglets and immediately (<24 h after birth) excised, trimmed to a desired thickness using an electric dermatome (Integra Life Sciences™, Padgett Instruments, NJ, USA) and frozen in liquid nitrogen vapour. Skin was then stored, for no longer than two weeks, at −20 °C until further use. Shaved skin samples, and Silescol® membranes, were pre-equilibrated in the receptor medium, phosphate buffered saline (PBS) pH 7.4 for 1 h before initiation of the experiments. A circular specimen of the skin was secured to the donor compartment of the diffusion cell using cynoacrylate adhesive (Loctite, Dublin, Ireland) with the *stratum corneum* side facing the donor compartment. Using a spring-activated applicator, as described previously (Donnelly et al., 2010a), MNs were inserted with an application force of 11.0 N/array into the centre of the skin. MNs were kept in place during the experiment by application of a non-adhesive putty material (BluTac®, Bostik Ltd., Leicester, UK) to their upper surface. With MN arrays in place, donor compartments were mounted onto the receptor compartments of the Franz cells. Using a long needle, samples (0.30 ml) were removed from the receptor compartment at defined time intervals and replaced with an equal volume of pre-warmed 0.1 M PBS pH 7.4. As a negative control, drug loaded patches (with the same drug loading but containing no MNs) were applied to skin using the spring-activated applicator at a force of 11.0 N/patch, and kept in place during the experiment by application of a non-adhesive putty material (BluTac®, Bostik Ltd., Leicester, UK). Sink conditions were maintained throughout all experiments. The concentrations of caffeine and lidocaine in the receiver medium were determined by HPLC and the concentrations of fluorescein sodium, methylene blue, metronidazole and theophylline were determined spectrophotometrically.

2.4. Pharmaceutical analysis of model drugs

Caffeine analysis was performed using RP-HPLC (Agilent 1200® Binary Pump, Agilent 1200®, Standard Autosampler, Agilent 1200®

Table 1
Actual loading of model drugs encapsulated throughout the entirety of the MN array matrix, *i.e.* total amount of drug contained within the MNs and the base plate upon which MNs are formed.

	Caffeine	Lidocaine HCl	Methylene Blue	Fluorescein sodium	Metronidazole	Theophylline
Amount (μg)	3100	7260	3500	3500	4800	3500

Variable Wavelength Detector, Agilent Technologies UK Ltd, Stockport, UK) with UV detection at 273 nm. Separation was achieved using a C_{18} (4.6 mm × 150 mm, 5 μm packing) Spherisorb® (Waters Associates, UK) analytical column fitted with a guard column of matching chemistry. The mobile phase consisted of an isocratic ratio of 90:10 of 0.52% v/v acetic acid aqueous solution and mixture of 50% acetonitrile and 50% tetrahydrofuran. The injection volume was 50 μl and elution was at a flow rate of 1 ml/min. The column was thermostated at 35 °C. The chromatographs obtained were analysed using Agilent ChemStation® Software B.02.01.

Lidocaine analysis was performed using RP-HPLC with UV detection at 265 nm. Separation was carried using C_{18} Bondapak™ (3.9 mm × 300 mm, 10 μm packing) analytical column fitted with a guard column of matching chemistry. The mobile phase consisted of 0.02 M phosphate buffer pH 6 and acetonitrile in the ratio 55:45. The injection volume was 20 μl and elution was at a flow rate of 1 ml/min. The chromatographs obtained were analysed using Agilent ChemStation® Software B.02.01.

Methylene blue, fluorescein sodium, metronidazole and theophylline were analysed using UV spectrophotometry (PowerWave XS Microplate Spectrophotometer, Bio-Tek, Winooski, USA) at wavelengths of 664 nm, 520 nm, 320 nm and 282 nm, respectively.

Least squares linear regression analysis and correlation analysis were performed on the calibration curves produced, enabling determination of the equations of the line and their coefficients of determination. To determine limits of detection (*LoD*) and limits of quantification (*LoQ*), an approach based on the standard deviation of the response and the slope of the representative calibration curve was employed, as described in the guidelines from ICH (47). The *LoD* of each method was determined as follows, using Eq. (1):

$$LoD = \frac{3.3\sigma}{S} \quad (1)$$

where σ is the standard deviation of the response (peak area) of the data used to construct the regression line and S is the slope of that line. Similarly, the *LoQ* was determined using Eq. (2):

$$LoQ = \frac{10\sigma}{S} \quad (2)$$

2.5. In vivo evaluation

Prior to experimentation, male Sprague-Dawley rats, weighing 315 ± 17 g, were acclimatised to laboratory conditions for a 7 day period. All animal experiments throughout this study were conducted according to the policy of the federation of European Laboratory Animal Science Associations and the European Convention for the protection of vertebrate animals used for experimental and other scientific purposes, with implementation of the principles of the 3Rs (replacement, reduction, refinement).

To prevent the animals' hair from interfering with dermal contact of MN arrays, animals were anaesthetised using gas anaesthesia (2–4% isoflurane in oxygen) and the hair covering the back and abdominal region removed using an electric hair clipper, 24 h before experimentation. Additionally, depilatory cream (Boots Expert®, The Boots Company PLC, Nottingham, UK) was used to remove any residual hair. A total of two methylene blue loaded soluble PMVE/MA MN arrays were inserted, using the spring activated applicator at a force of 11.0 N per array, at a distal site on the animal's back. In order to keep the MN array in place for a 24 h period, and provide occlusion of the administration site, a silicone sheet was applied on top of the MN base plate, as described previously (Migalska et al., 2011). The MN patch was then further secured to the skin site using elasticated adhesive support tape (The Boots Company PLC, Nottingham, UK).

After application of MN arrays, a 0.25 ml aliquot of blood drawn from the tail vein was collected into heparinised tubes (Microvette CB® 300, Sarstedt, Leicester, UK) at defined time intervals over a 24 h period. Plasma samples were obtained by centrifuging the collected blood samples at 10,000 rpm for 10 min. All samples were analysed spectrophotometrically within 2 h of collection at a wavelength of 664 nm. As a negative control, methylene blue loaded patches, of the same composition of the MN formulations but containing no MNs on their surface, were applied to the rats and blood samples collected using the same procedure described above.

At the end of the 24 h study period, the animals were sacrificed *via* carbon dioxide asphyxiation and the MN base plate was carefully removed from the skin surface and dissolved in 20 ml of PBS pH 7.4. The amount of methylene blue extracted from the MN base plate was quantified spectrophotometrically, as described above. Furthermore, a scalpel was used to excise the skin tissue exposed to the MN array (approximately 1.2 × 1.2 × 0.8 mm). This tissue was then flash frozen in a liquid nitrogen atmosphere prior to tissue sectioning to aid in the solubilisation of the skin tissue. Sections of frozen tissue were mounted on the stage of a cryostatic microtome (Leica CM1900-1-1 cryostatic microtome, Leica Microsystems, Nussloch, Germany) using tissue embedding fluid. The microtome environment and stage were operated at −25 °C. Frozen tissue sections were positioned so that their upper surfaces, to which MNs had been applied, were parallel to the slicing motion of the blade (Donnelly et al., 2010b). Slice thickness was set at 200 μm, and consecutive slices were taken and placed into the same sample vial. This procedure was repeated until the entire section was sliced. To dissolve the skin tissue, 5.0 ml of NCS II Tissue solubiliser (Amersham Canada Ltd, Ontorio, Canada) was added to the sample vial. The vial was sonicated for 12 h at 40 °C. The amount of methylene blue extracted was quantified spectrophotometrically, as described above.

2.6. Optical coherence tomography

The penetration characteristics, and subsequent in-skin dissolution kinetics, of methylene blue loaded PMVE/MA MN arrays following application, using the spring activated applicator at a force of 11.0 N per array, to each of the skin model membranes, within the Franz cell set-up used for the *in vitro* permeation studies, was determined using optical coherence tomography (OCT) (VivoSight® high resolution OCT scanner with handheld probe, Michelson Diagnostics Ltd, Kent, UK), as described previously (Donnelly et al., 2010a). Furthermore, OCT was used to visualise the penetration characteristics, and in-skin dissolution profile, of methylene blue loaded PMVE/MA MN arrays following application to male Sprague-Dawley rats *in vivo*. The swept-source Fourier domain OCT system has a laser centre wavelength of 1305.0 ± 15.0 nm, facilitating real time high resolution imaging of the upper skin layers (7.5 μm lateral and 10.0 μm vertical resolution). The skin model was scanned at a rate of up to 15 B-scans (2D cross-sectional scans) per second (scan width = 2.0 mm). 2D images were analysed using the imaging software ImageJ®. The

Table 2
Calibration curves properties of caffeine, lidocaine HCl, methylene blue, fluorescein sodium, metronidazole and theophylline as determined by linear regression and correlation analysis, *LoD* and *LoQ*, and linear concentration range.

Drug	Slope	*y*-Intercept	r^2	*LoD* (μg/ml)	*LoQ* (μg/ml)	Linear range (μg/ml)
Caffeine	43.66	−2.18	0.9986	0.16	0.48	2–20
Lidocaine HCl	0.48	0.22	0.9999	2.21	6.71	10–100
Methylene blue	0.14	0.05	0.9945	0.48	1.46	1–9
Fluorescein sodium	0.12	0.01	0.9999	0.06	0.19	1–9
Metronidazole	0.047	0.001	0.9973	0.35	1.17	1–30
Theophylline	0.027	−0.021	0.9991	1.24	3.75	2.5–30

scale of the image files obtained was 1 pixel = 4.2 μm, thus allowing accurate measurements of the depth of MN penetration, the width of the pore created, and the distance between the MN base plate and the *stratum corneum*. To allow differentiation between MN and skin model layers false colours were applied using Ability Photopaint® Version 4.14 (Ability Plus Software Ltd, Crawley, UK). In all instances, experiments were performed in triplicate, and >5 MN measured for each replicate.

2.7. Statistical analysis

Where appropriate, data were analysed using a one-way analysis of variance (ANOVA), with *post hoc* comparisons performed using Tukey's HSD test. In all cases, $p < 0.05$ denoted significance.

3. Results

In order to assess the effect of the skin model on MN-mediated drug delivery, three model membranes, namely a synthetic membrane, Silescol® (75 μm thick) and natural membranes dermatomed (300–350 μm) and full-thickness (700–750 μm) neonatal porcine skin were employed. Caffeine, lidocaine HCl, methylene blue, fluorescein sodium metronidazole and theophylline were all successfully incorporated at defined loadings into the structure of MNs prepared from aqueous blends of 20% w/w PMVE/MA. Manufactured polymeric MNs encapsulating model compounds were characterized by similar mechanical strength in comparison to non-loaded MNs (data not shown).

Table 2 shows calibration curve properties for analytical methods of all tested compounds. The calibration curve of caffeine, lidocaine HCl, methylene blue, fluorescein sodium, metronidazole and theophylline were found to be linear in the range of 2–20, 10–100, 1–9, 1–9, 1–30, and 2.5–30 μg/ml, respectively. The developed assays were found to be reproducible, with good precision and accuracy. The methods specificity investigations revealed that, under the assays conditions described above no interference from the MN matrix was observed.

In vitro permeation studies revealed that transport of all tested compounds across model membranes was markedly increased in each case when MNs prepared from aqueous blends of 20% PMVE/MA were employed (Table 3).

Fig. 1(A–F) presents permeation profiles of model drugs released from polymeric MNs across Silescol®, dermatomed and full-thickness neonatal porcine skin.

The enhancement effect of MNs on transport of model compounds across Silescol® membrane was found to be relatively low. The use of MNs loaded with fluorescein sodium, methylene blue, and theophylline facilitated their delivery only by 2.79-fold, 3.82-fold, and 3.05-fold, respectively, in comparison to the passive diffusion from drug loaded control patches containing no MNs (Table 3). Similarly, MN-mediated transport of caffeine, lidocaine HCl, and metronidazole was improved only by 1.84-fold, 3.25-fold, and 1.91-fold, respectively, when compared to the permeation across an intact Silescol® membrane (Table 3). Whilst MN application to the Silescol® membrane resulted in detectable levels of model compounds within the first 15 min, this rapid release was not followed by a sustained marked increase in the cumulative percentage permeation throughout the 24 h experimental period.

The greatest extent of MN mediated drug permeation was observed when dermatomed (300–350 μm) neonatal porcine skin was used as the model skin membrane. In particular, the application

Table 3
Cumulative amount of model drugs permeated across different skin model membranes after 24 h (means ± SD, $n \geq 5$).

Drug	Cumulative amount permeated after 24 h (μg)		
	Skin model		
	Silescol® (75 μm)	300–350 μm	700–750 μm
Caffeine			
Control	135.69 ± 40.58	136.40 ± 23.17	81.44 ± 15.24
MN array	248.92 ± 96.17	1833.74 ± 302.33	1408.56 ± 133.69
Lidocaine HCl			
Control	ND[a]	150.96 ± 35.07	71.81 ± 21.12
MN array	236.35 ± 36.01	2848.26 ± 652.11	2024.25 ± 281.63
Methylene blue			
Control	34.07 ± 5.36	229.50 ± 15.42	136.41 ± 13.76
MN array	129.94 ± 9.13	2361.84 ± 108.31	1661.45 ± 96.52
Fluorescein sodium			
Control	25.66 ± 1.13	142.80 ± 11.79	100.15 ± 4.96
MN array	71.42 ± 14.78	1965.25 ± 179.61	1522.57 ± 104.25
Metronidazole			
Control	67.63 ± 14.51	188.12 ± 81.06	97.44 ± 8.91
MN array	129.37 ± 30.02	1102.28 ± 101.51	798.62 ± 106.83
Theophylline			
Control	85.16 ± 12.61	231.70 ± 48.36	146.73 ± 20.02
MN array	259.75 ± 63.04	2717.05 ± 121.82	1622.61 ± 113.10

[a] ND = not detectable.

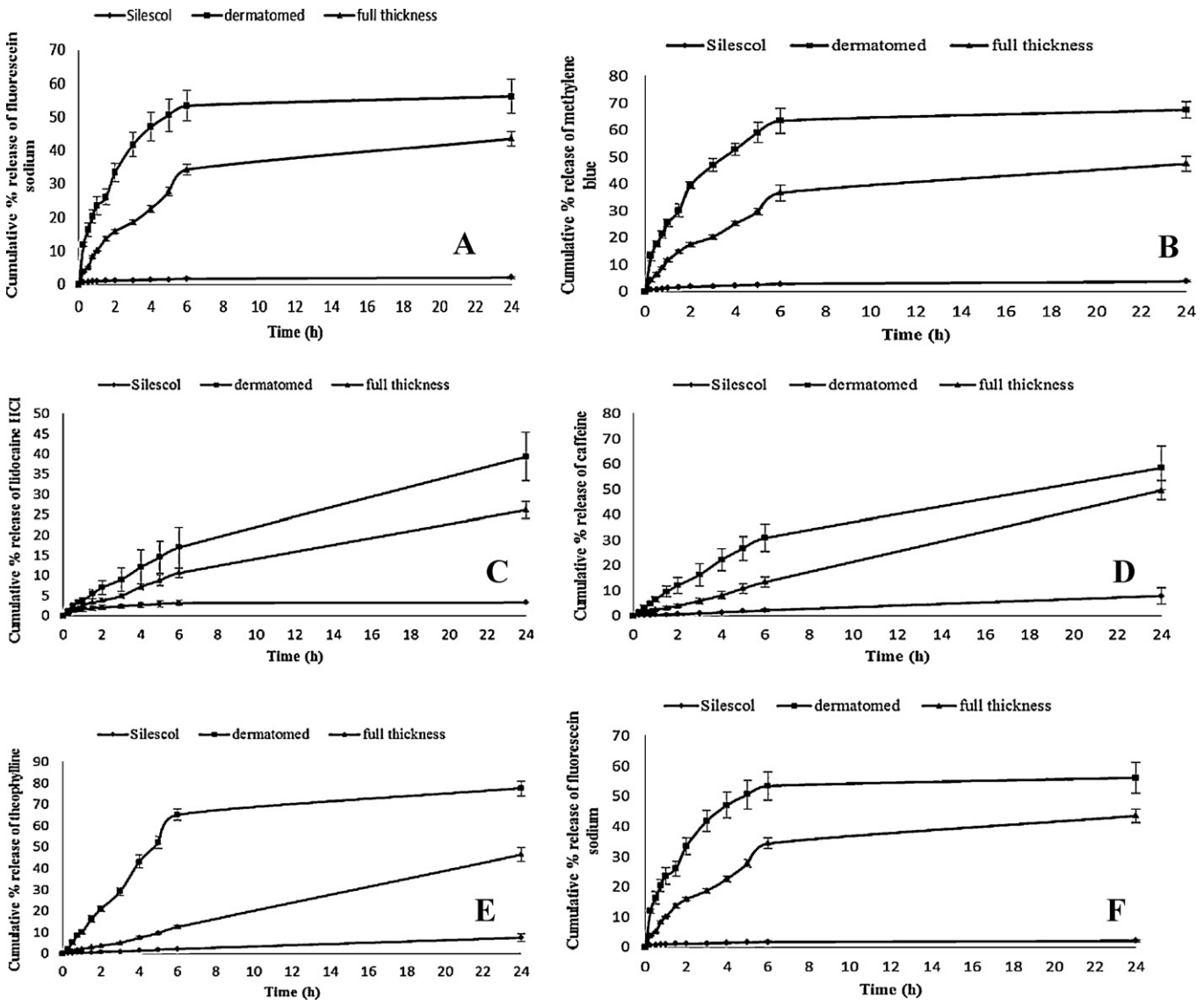

Fig. 1. Cumulative percentage permeation of (A) fluorescein sodium, (B), methylene blue, (C) lidocaine HCl, (D) caffeine, (E) theophylline, and (F) metronidazole across Silescol® membrane, dermatomed and full-thickness neonatal porcine skin (mean ± SD, $n \geq 5$).

of MNs encapsulating fluorescein sodium, methylene blue, and theophylline resulted in cumulative percentage permeation of approximately 56%, 67%, and 77% 24 h after MN application, respectively (Fig. 1). When MNs loaded with caffeine, lidocaine HCl and metronidazole were applied, the cumulative percentage permeation was found to be approximately 59%, 39% and 23%, respectively (Fig. 1). It was observed that there was a gradual and sustained increase in the extent of drug permeation across dermatomed (300–350 μm) neonatal porcine skin over the 24 h period. In comparison, the passive permeation across non MN treated dermatomed (300–350 μm) neonatal porcine skin resulted in mean cumulative percentage permeations at 24 h of approximately 4.08%, 6.55%, 6.62%, 4.40%, 2.08% and 3.92% for fluorescein sodium, methylene blue, theophylline, caffeine, lidocaine HCl and metronidazole, respectively (Table 3). As such, when MN were used to percutaneously deliver fluorescein sodium, methylene blue, and theophylline across dermatomed (300–350 μm) neonatal porcine skin, cumulative percentage permeations were increased by 13.76-fold, 10.30-fold, and 11.73-fold, respectively. Similarly, MN-mediated transport of caffeine, lidocaine HCl and metronidazole was improved by 13.44-fold, 18.86-fold, and 5.86-fold, respectively, when compared to the permeation across intact skin.

Table 4 shows the depth of MN penetration achieved following the application of methylene blue loaded MN arrays to the back of the rats during the *in vivo* investigations. It was found that, following application, MNs penetrated to a depth of approximately 430 μm, creating a pore within the *stratum corneum* of approximately 224 μm. As can be appreciated from Fig. 2, the MN does not penetrate the skin in its entirety, with a clear gap evident between the skin surface and the MN base plate of approximately 166 μm. This observation is consistent with our previous reported findings (Donnelly et al., 2010a, 2011).

Table 4
OCT assessment of MN penetration following application to rats *in vivo* (means ± SD, $n > 15$).

MN penetration depth (μm)	Pore width (μm)	Base plate/*SC* distance (μm)
429.66 ± 6.37	224.08 ± 4.62	166.36 ± 5.88

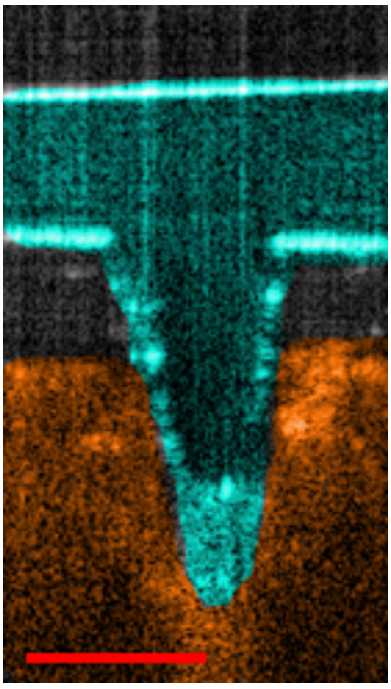

Fig. 2. Representative OCT image showing the penetration of a MN array into rat skin following application *in vivo*. Scale bar represents a length of 300 μm.

Fig. 3 highlights the plasma concentration profile of methylene blue following application of methylene blue loaded soluble PMVE/MA MN arrays in a rat model *in vivo*. It was found that MN application significantly increased the percutaneous penetration of methylene blue in comparison to a control methylene blue loaded patch, of the same composition of the MN arrays but containing no MNs. In particular, detectable levels of methylene blue reached the systemic circulation within 30 min after MN application and gradually increased, resulting in a maximal methylene blue plasma concentration of 100.02 ± 13.19 μg/ml 24 h after MN application. This is in comparison to the maximum methylene blue plasma concentration of 2.62 ± 0.65 μg/ml found 24 h after the application of the control patch.

At the end of the 24 h experimental period, the MN base formulation was removed and a biopsy of the skin site obtained, thus enabling extraction and quantification of the amount of methylene blue remaining within the formulation and dermal tissue. It can be seen in Table 5 that approximately 24% and 10% of the methylene blue loaded into the MN array was retained within the MN base and the excised skin tissue 24 h after MN application, respectively.

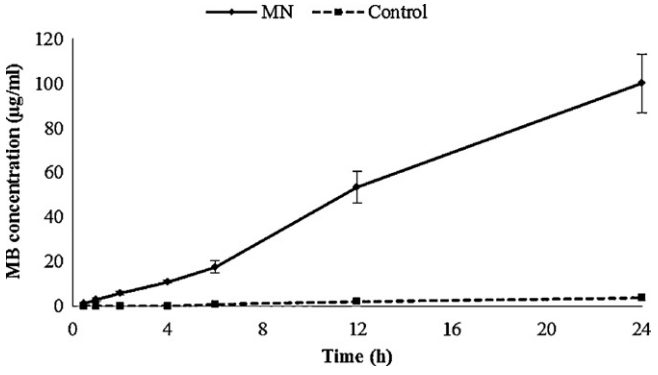

Fig. 3. *In vivo* plasma concentration profile of methylene blue following the application of methylene blue loaded soluble MN arrays or control patches (means ± SD, $n = 5$).

Table 5
Recovery of methylene blue following MN array removal after 24 h period of application to rat skin *in vivo* (means ± SD, $n = 3$).

	% of MB originally loaded into MN array
MN–base	23.59 ± 2.32
Excised skin	9.65 ± 1.73

As such, this would suggest that approximately 66% of the available of methylene blue loaded into the MN array was delivered across the skin during the course of the 24 h application period, which is remarkably similar to the % cumulative amount of methylene blue that permeated across MN treated dermatomed neonatal porcine skin during the *in vitro* investigations (Fig. 1).Optical coherence tomography was utilised to evaluate the rate of MN dissolution following application to each of the model skin membranes within the *in vitro* Franz cell set-up, in addition to the dissolution profile of MNs inserted into rat skin *in vivo*. As shown in Table 6, the methylene blue loaded MN arrays rapidly dissolved within the first 15 min following application to rat skin, dermatomed and full thickness neonatal porcine skin.Interestingly, however, whilst visual inspection during the *in vitro* investigations revealed that MN penetrate across the entire thickness (75 μm) of the Silescol® following application with the spring activated applicator, the use of OCT highlighted that, the highly elastic nature of the Silescol® membrane caused the MN array to quite quickly (<1 min) retract, such that the MNs did not actually reside within the created micropores (Fig. 4).

Fig. 5 shows representative OCT images of the dissolution of methylene blue loaded MNs following application to rat skin *in vivo*.

Whilst, following MN application, a clear gap of approximately 166 μm is evident between the skin surface and the MN base plate (Fig. 5A), OCT analysis led to an interesting observation. In particular, the process of MN dissolution (Fig. 5B–E) was accompanied by an uptake of fluid into the MN base plate, leading to its subsequent swelling and increased adhesion to the skin surface. This process of improved bioadhesion may be of importance in enabling sustained drug delivery across the microporated skin following complete MN dissolution.

Figs. 6 and 7 show representative OCT images of methylene blue loaded MNs dissolving following application to dermatomed and full thickness neonatal porcine skin, respectively.

Table 6
OCT - led evaluation of methylene blue loaded MN dissolution following application to each of the model skin membranes. (means ± SD, $n \geq 15$). *ND = not determinable.

Skin model			
Rat skin *in vivo*		Silescol®	
Time (min)	MN height remaining in skin (μm)	Time (min)	MN height remaining in skin (μm)
0	429.7 ± 6.4	0	ND
3	266.8 ± 7.2	3	ND
5	155.3 ± 9.93	5	ND
7	100.5 ± 7.0	7	ND
10	81.1 ± 5.6	10	ND
15	49.8 ± 3.1	15	ND
Dermatomed neonatal porcine skin		Full thickness skin	
Time (min)	MN height remaining in skin (μm)	Time (min)	MN height remaining in skin (μm)
0	≥350.0	0	466.3 ± 4.9
3	200.6 ± 5.2	3	275.9 ± 10.9
5	149.4 ± 6.7	5	203.1 ± 7.9
7	92.7 ± 4.7	7	132.2 ± 9.2
10	75.8 ± 6.4	10	92.33 ± 5.2
15	51.5 ± 4.1	15	51.4 ± 6.6

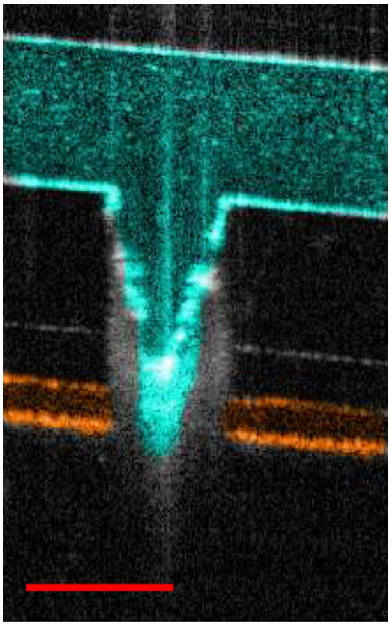

Fig. 4. Representative OCT image highlighting the inability of the MN array (in blue) to reside within the created micropore following application to a Silescol® membrane (in brown). Scale bar represents a length of 300 μm.

4. Discussion

In the field of transdermal drug delivery, the Franz diffusion cell is the most commonly employed set-up for *in vitro* investigations of drug release from formulations. Skin samples of varying thickness have been used as the diffusional barrier to evaluate MN mediated drug delivery (Park et al., 2006; Verbaan et al., 2007; Donnelly et al., 2010a). Synthetic membranes have also been widely used as an alternative model of the major skin barrier – the *stratum corneum* (*SC*) – during drug permeation investigations (Coulman et al., 2009; Williams, 2003). The use of such membranes has been proposed due to their accessible and affordable nature, and, given that they do not require complex pre-treatment or inconvenient transport or storage conditions, they may potentially reduce the variability related to the use of animal or human skin (Huong et al., 2009). In the current study, we investigated the effect of skin model, employing a widely used synthetic membrane (Silescol®) and neonatal porcine skin of defined thicknesses, on the percutaneous transport of model drugs released from dissolving polymeric MNs.

Classically, the primary barrier to the transdermal delivery of drug molecules is posed by the highly lipophilic uppermost layer of the skin – the *SC*. However, MNs are specifically designed to mechanically by-pass the *SC* barrier and deliver drugs through the epidermis to the capillary bed below the epidermal–dermal junction. Therefore, since the *SC* had been by-passed, when considering MN mediated transdermal drug administration, solute diffusion across the epidermis/dermis to the dermal capillary bed is believed to be the rate limiting step (Fukushima et al., 2010).

In vitro skin permeation experiments are typically employed to optimise formulation design for enhanced percutaneous drug delivery (Friend, 1992). Accordingly, drug permeation across *in vitro* skin models should allow some prediction of *in vivo* percutaneous absorption. However, under *in vitro* conditions, an active microcirculation is absent. This means that the distance from the skin/membrane surface to its interface with the receptor medium will present the barrier to drug permeation. In living skin, the distance from the *SC* to the dermal microvasculature, where most

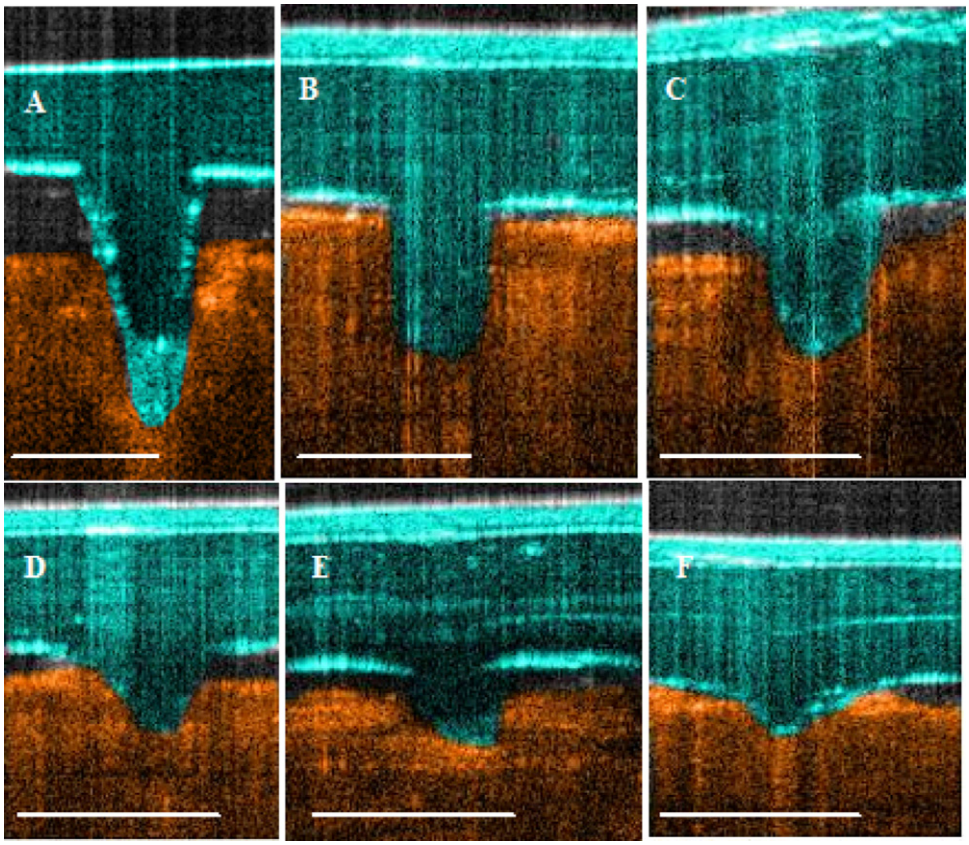

Fig. 5. Representative OCT images of methylene blue loaded MN dissolving following application to rat skin *in vivo*. (A) Time = 0 min, (B) time = 3 min, (C) time = 5 min, (D) time = 7 min, (E) time = 10 min, (F) time = 15 min. Scale bar represents a length of 300 μm.

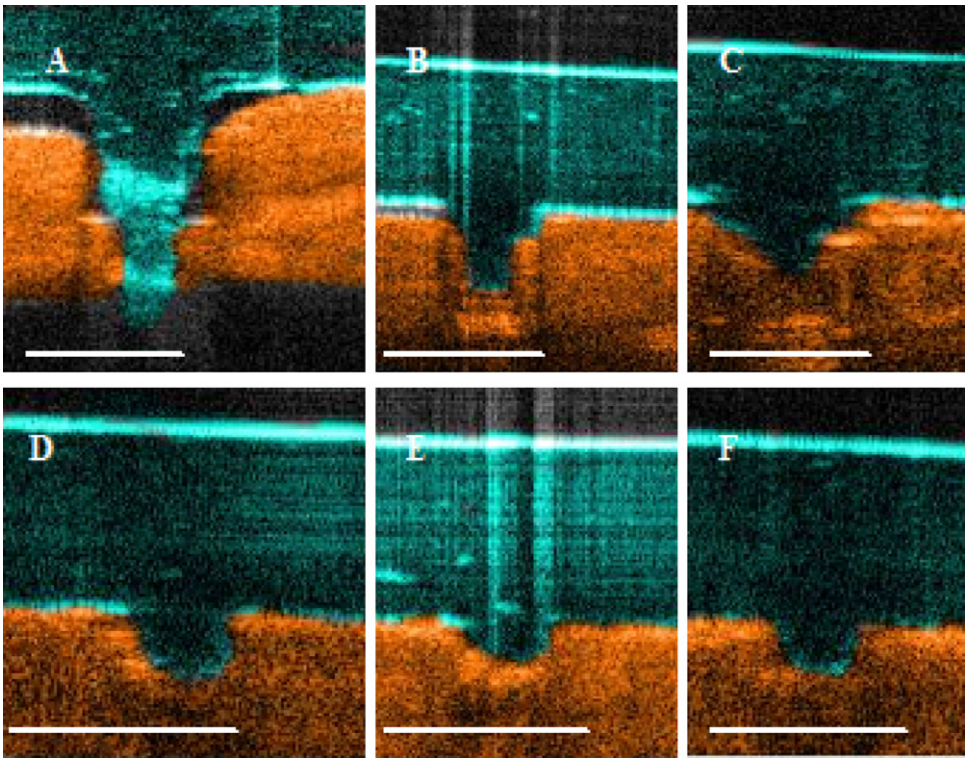

Fig. 6. Representative OCT images of methylene blue loaded MNs dissolving following application to dermatomed neonatal porcine skin *in vitro*. (A) Time = 0 min, (B) time = 3 min, (C) time = 5 min, (D) time = 7 min, (E) time = 10 min, (F) time = 15 min. Scale bar represents a length of 300 μm.

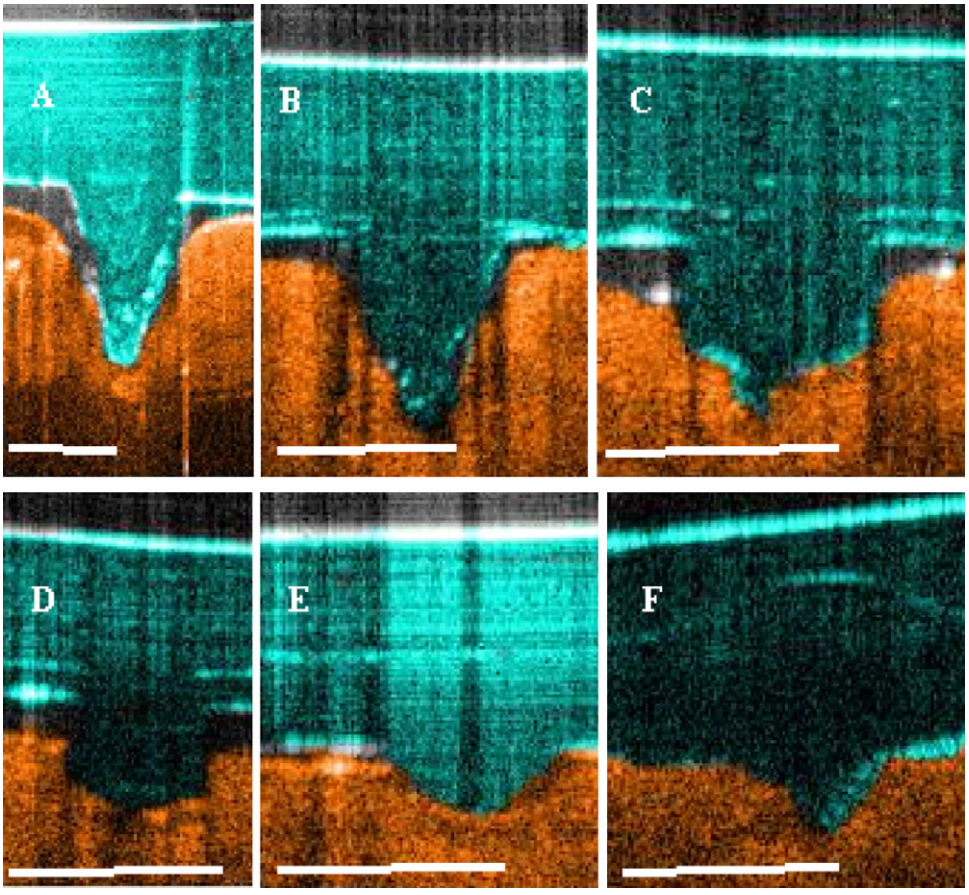

Fig. 7. Representative OCT images of methylene blue loaded MNs following application to full thickness neonatal porcine skin *in vitro*. (A) Time = 0 min, (B) time = 3 min, (C) time = 5 min, (D) time = 7 min, (E) time = 10 min, (F) time = 15 min. Scale bar represents a length of 300 μm.

drugs are absorbed, is of the order of 200–400 μm (Scheuplein, 1967). Therefore, an important aspect of proper design of *in vitro* permeability experiments is careful consideration of the membrane used to model *in vivo* skin conditions (Friend, 1992). To date, no such discussion has taken place for MN-mediated delivery. The development of dissolvable polymeric MN arrays which, upon contact with the skin interstitial fluid, will either dissolve or degrade to release their drug cargo *in situ*, requires additional factors to be considered when designing *in vitro* permeation experiments. Ideally, the model membrane chosen as a representation of the skin barrier *in vitro* should mimic the depth of MN penetration, the adhesion of the MN baseplate to the skin surface, the MN dissolution/degradation rate and subsequent drug release achieved in an *in vivo* scenario. Furthermore, given that in most instances MN length may be greater than the thickness of the skin membrane employed as a barrier, then a proportion of the MN may be in direct contact with the receiver medium. Consequently, it will be important to ensure that selection of receiver medium composition does not substantially overestimate the rate of MN dissolution and, therefore, the rate of drug release within skin.

The first stage of our investigations utilised a synthetic hydrophobic membrane, Silescol® of a thickness of 75 μm, as the representation of the primary skin barrier to drug transport. It was found that, when Silescol® was used, MN mediated transport of all model compounds was only modestly enhanced (between 2 and 4-fold, $p < 0.01$ in all cases) in comparison to their passive permeation from drug loaded patches and was the lowest in comparison to the other skin models employed. Whilst visual inspection of the Silescol® membrane following MN application highlighted that the MN did create micropores that breached the entire thickness of the membrane, the use of OCT within this study revealed that the high elasticity of this membrane caused the MNs to quite quickly (<1 min following MN application) retract, such that the MNs did not actually reside within created micropores (Fig. 4). As a result, the permeation of drugs across this membrane from the MN array was akin to a "poke and patch" technique (Garland et al., 2011). In this instance, the hygroscopic nature of the PMVE/MA formulation enabled the surface-residing MN array to absorb fluid from the Franz cell receiver compartment, leading to hydration of the MN array with subsequent liberation and release of the incorporated drug. We have previously shown that such a phenomenon does not occur following the application of PMVE/MA MNs to a human volunteer *in vivo* (Donnelly et al., 2011). As such, the use of Silescol® membrane does not accurately reflect the penetration and adhesion of PMVE/MA MNs achieved *in vivo* and may, therefore, lead to an under-estimation of the drug release profile achieved from *in situ* dissolvable polymeric MN devices.

As discussed above, the effective barrier distance that MN mediated molecules must traverse to reach the systemic circulation is within the region of 200–400 μm (Scheuplein, 1967). Consequently, from the point of view of *in vitro* experimentation, the performance of MN devices could be potentially better predicted using a skin model representing this epidermal and dermal barrier. However, we have previously shown that PMVE/MA MNs of 600 μm height penetrate to a depth of approximately 460 μm when applied to neonatal porcine skin at a force of 11.0 N per array (Donnelly et al., 2010a), meaning that a proportion of the MN will be in direct contact with the receiver medium when using epidermal/upper dermal representations of the skin barrier. As such, due consideration of the effect that the receiver medium may have upon the rate of MN dissolution should be taken into account. In this respect, dermatomed neonatal porcine skin (300–350 μm thick) was used to represent the approximate distance from the skin surface to the dermal microcirculation and full thickness neonatal porcine skin (700–750 μm) was used as a skin model where no portion of the penetrated MN would reside within the receiver medium. Our results revealed that, for the wide range of drug molecules investigated, the use of dermatomed neonatal porcine skin as the model membrane resulted in the greatest extent of MN-mediated percutaneous permeation in comparison to full thickness skin (Fig. 1) ($p < 0.01$ in all cases). Given that the diffusion of molecules across epidermis–dermis will be the rate-limiting step in absorption of MN-delivered compounds (Fukushima et al., 2010), this may be attributable to the increased diffusional path-length associated with the use of full thickness skin (Williams, 2003; Banga, 2011). Indeed, it has recently been shown that the percutaneous delivery of insulin *in vivo* was significantly enhanced when both the *SC* and viable epidermis, rather than just the *SC*, were removed (Andrews et al., 2011). This suggests that there may well be non-*SC* barriers to the MN-mediated transport of molecules across the skin that need to be considered, perhaps on a case-by-case basis, depending on drug physicochemical properties.

There was no significant difference between the rate of MN dissolution following application to dermatomed or full thickness neonatal porcine skin. In both cases, the MNs rapidly dissolved following skin insertion, with complete dissolution achieved approximately 15 min after MN application. Unlike the permeation profile observed across the Silescol® membrane, there was a steady increase in the amount of drug delivered across both types of neonatal porcine skin throughout the 24 h study period (Fig. 1). This suggest that, after complete MN dissolution, the created microchannels within the skin remain open under the occlusive conditions employed (Kalluri and Banga, 2011), thus facilitating continued hydration of the MN base plate and improved MN-skin adhesion with subsequent continued diffusion of the drug encapsulated within the MN base plate (Lee et al., 2008).

Application of methylene blue-loaded MN arrays to the skin of male Sprague-Dawley rats *in vivo* markedly increased the percutaneous delivery of methylene blue in comparison to that achieved across non-MN treated skin. Furthermore, the drug plasma level profile obtained indicated that MN application resulted in a sustained delivery of methylene blue over the 24 h study period, with the rate of absorption being greater than the rate of methylene blue excretion. This suggests that, although the MNs rapidly dissolve within 15 min after application (Fig. 5), the hygroscopic nature of the PMVE/MA MN arrays is such that sufficient interstitial fluid is absorbed through the open micropores to allow hydration of the MN base plate, leading to increased adhesion to the skin surface and subsequent liberation and diffusion of methylene blue incorporated throughout the MN base plate matrix. Interestingly, mass balance analysis revealed that approximately 67% of the available methylene blue loaded into the MN device was delivered across the skin over the course of the 24 h period, which is very similar to the cumulative percentage permeation of methylene blue obtained when using dermatomed neonatal porcine skin as a model membrane during the *in vitro* investigations. Human volunteer studies are now the necessary next step moving forwards.

5. Conclusion

This study confirmed the influence of choice of *in vitro* experimental conditions on the rate and extent of permeation of a wide range of small hydrophilic model compounds from dissolvable polymeric MN arrays. The results of the present study suggest that synthetic membranes should be employed with caution when evaluating drug release from MN devices that are designed to deposit their drug loadings locally *via* a dissolution or degradation whilst *in situ*. Ideally a model skin membrane should mimic the depth of MN penetration, MN adhesion to the skin surface, rate of MN dissolution and subsequent drug release achieved following MN application to skin *in vivo*. In this respect, it appears that, as long as

the composition of the receiver medium itself does not significantly affect the dissolution profile of such MN devices, then dermatomed neonatal porcine skin may be a more approximate measure of the *in vivo* performance of drug-loaded dissolvable polymeric MN arrays. Further discussion and debate within the MN and transdermal communities is now necessary to enable standardisation of experimental protocols to aid in the successful progression of promising MN-based drug delivery technologies through to commercialisation. Ultimately, significant industrial investment will be required for controlled human volunteer trials with associated *in vitro*/*in vivo* correlations.

Acknowledgements

This study was supported by BBSRC grant numbers BB/FOF/287 and BB/E020534/1 and Wellcome Trust grant number WT094085MA.

References

Ameri, M., Fan, S.C., Maa, Y.F., 2010. Parathyroid hormone PTH(1–34) formulation that enables uniform coating on a novel transdermal microprojection delivery system. Pharm. Res. 27, 303–313.

Andrews, S., Lee, J.W., Choi, S.O., Prausnitz, M.R., 2011. Transdermal insulin delivery using microdermabrasion. Pharm. Res. 28, 2110–2118.

Badkar, A., Smith, A., Eppstein, J., Banga, A., 2007. Transdermal delivery of interferon alpha-2B using microporation and iontophoresis in hairless rats. Pharm. Res. 24, 1389–1395.

Bal, S.M., Caussin, J., Pavel, S., Bouwstra, J.A., 2008. In vivo assessment of safety microneedle arrays in human skin. Eur. J. Pharm. Sci. 35, 193–202.

Banga, A.K., 2006. Therapeutic Peptides and Proteins: Formulation, Processing and Delivery Systems. CRC Press, Boca Raton.

Banga, A.J., 2011. Transdermal and Intradermal Delivery of Therapeutic Agents. CRC Press, Boca Raton.

Chu, L., Choi, S., Prausnitz, M., 2010. Fabrication of dissolving polymer microneedles for controlled drug encapsulation and delivery: bubble and pedestal microneedle designs J. Pharm. Sci. 99, 4228–4238.

Cormier, M., Johnson, B., Ameri, M., Nyam, K., Libiran, L., Zhang, D., Daddona, P., 2004. Transdermal delivery of desmopressin using a coated microneedle array patch system. J. Control. Release 97, 503–511.

Coulman, S.A., Anstey, A., Gateley, C., Morrissey, A., McLoughlin, P., Allender, C., Birchall, J.C., 2009. Microneedle mediated delivery of nanoparticles into human skin. Int. J. Pharm. 366, 190–200.

Donnelly, R.F., Garland, M.J., Morrow, D.I.J., Migalska, K., Singh, T.R.R., Majithiya, R., Woolfson, A.D., 2010a. Optical coherence tomography is a valuable tool in the study of the effects of microneedle geometry on skin penetration characteristics and in-skin dissolution. J. Control. Release 147, 333–341.

Donnelly, R.F., Morrow, D.I.J., Fay, F., Scott, C.J., Abdelghany, S., Singh, T.R.R., Garland, M.J., Woolfson, A.D., 2010b. Microneedle-mediated intradermal nanoparticle delivery: potential for enhanced local administration of hydrophobic pre-formed photosensitisers. Photodiag. Photodynam. Ther. 7, 222–231.

Donnelly, R.F., Majithiya, R., Singh, T.R.R., Morrow, D.I.J., Garland, M.J., Demir, Y.K., Migalska, K., Ryan, E., Gillen, D., Scott, C., Woolfson, A.D., 2011. Design, optimization and characterization of polymeric microneedle arrays prepared by a novel laser-based micromoulding technique. Pharm. Res. 28, 41–57.

Friend, D.R., 1992. In vitro skin permeation techniques. J. Control. Release 18, 235–248.

Fujiwara, A., Hinokitani, T., Goto, K., Arai, T., 2005. Partial ablation of porcine stratum corneum by argon-fluoride excimer laser to enhance transdermal drug permeability. Laser Med. Sci. 19, 210–217.

Fukushima, K., Ise, A., Morita, H., Hasegawa, R., Ito, Y., Sugioka, N., Takada, K., 2010. Two-layered dissolving microneedles for percutaneous delivery of peptide/protein drugs in rats. Pharm. Res., http://dx.doi.org/10.1007/s11095-010-0097-7.

Gardeniers, H., Luttge, R., Berenschot, E., de Boer, M., Yeshurun, S., Hefetz, M., van't Oever, R., van den Berg, A., 2003. Silicon micromachined hollow microneedles for transdermal liquid transport. J. Microelectromech. Syst. 12, 855–862.

Garland, M.J., Migalska, K., Mahmood, T.M.T., Singh, T.R.R., Woolfson, A.D., Donnelly, R.F., 2011. Microneedle arrays as medical devices for enhanced transdermal drug delivery. Expert Rev. Med. Devices 8, 459–482.

Gupta, H., Sharma, A., 2009. Recent trends in protein and peptide drug delivery systems. Asian J. Pharm. 3, 69–75.

Henry, S., McAllister, D.V., Allen, M.G., Prausnitz, M.R., 1998. Microfabricated microneedles: a novel approach to transdermal drug delivery. J. Pharm. Sci. 87, 922–925.

Huong, S., Bun, H., Fourneron, J., Reynier, J., Andrieu, V., 2009. Use of various models for *in vitro* percutaneous absorption studies of ultraviolet filters. Skin Res. Technol. 15, 253–261.

Ito, Y., Yoshmitsu, J., Shiroyama, K., Sugioka, N., Takada, K., 2006. Self-dissolving microneedles for the percutaneous absorption of EPO in mice. Drug Target. 14, 255–261.

Jiang, J., Moore, J.S., Henry, F., Prausnitz, M., 2009. Intrascleral drug delivery to the eye using hollow microneedles. Pharm. Res. 26, 395–403.

Kalluri, H., Banga, A.J., 2011. Formation and closure of microchannels in skin following microporation. Pharm. Res. 28, 82–94.

Karande, P., Jain, A., Mitragotri, S., 2004. Discovery of transdermal penetration enhancers by high-throughput screening. Nat. Biotechnol. 22, 192–197.

Kaushik, S., Allen, H., Donald, D., McAllister, D., Smitra, S., Allen, M., Prausnitz, M., 2001. Lack of pain associated with microfabricated microneedles. Anesth. Analg. 92, 502–504.

Kolli, C., Banga, A., 2008. Characterization of solid maltose microneedles and their use for transdermal delivery. Pharm. Res. 25, 104–113.

Lee, J.W., Park, H., Prausnitz, M.R., 2008. Dissolving microneedles for transdermal drug delivery. Biomaterials 29, 2113–2124.

Li, G., Badkar, A., Nema, S., Kolli, C.S., Banga, A.K., 2009. *In vitro* transdermal delivery of therapeutic antibodies using maltose microneedles. Int. J. Pharm. 368, 109–115.

Martanto, W., Davis, S.P., Holiday, N.R., Wang, J., Gill, H., Prausnitz, M.R., 2004. Transdermal delivery of insulin using microneedles *in vivo*. Pharm. Res. 21, 947–952.

Matriano, J.A., Cormier, M., Johnson, J., Young, W.A., Buttery, M., Nyam, K., Daddona, P.E., 2002. Macroflux microprojection array patch technology: a new and efficient approach for intracutaneous immunization. Pharm. Res. 19, 63–70.

McAllister, D., Wang, P., Davis, S., Park, J., Canatella, P., Allen, M., Prausnitz, M., 2003. Microfabricated needles for transdermal delivery of macromolecules and nanoparticles: fabrication methods and transport studies. PNAS 100, 13755–13760.

Medi, B.M., Singh, J., 2003. Electronically facilitated transdermal delivery of human parathyroid hormone. Int. J. Pharm. 263, 25–33.

Migalska, K., Morrow, D.I.J., Garland, M.J., Thakur, R., Woolfson, A.D., Donnelly, R.F., 2011. Laser-engineered dissolving microneedle arrays for transdermal macromolecular drug delivery. Pharm. Res. 28, 1919–1930.

Park, J.H., Allen, M.G., Prausnitz, M.R., 2005. Biodegradable polymer microneedles: fabrication, mechanics and transdermal drug delivery. J. Control. Release 104, 51–66.

Park, J.H., Allen, M.G., Prausnitz, M.R., 2006. Polymer microneedles for controlled-release drug delivery. Pharm. Res. 23, 1008–1019.

Park, E., Werner, J., Smith, N., 2007. Ultrasound mediated transdermal insulin delivery in pigs using a lightweight transducer. Pharm. Res. 24, 1396–1401.

Prausnitz, M.R., 2004. Microneedles for transdermal drug delivery. Adv. Drug Deliv. Rev. 56, 581–587.

Roxhed, N., Samel, B., Nordquist, L., Griss, P., Stemme, G., 2008. Painless drug delivery through microneedle-based transdermal patches featuring active infusion. IEEE Trans. Biomed. Eng. 55, 1063–1071.

Scheuplein, R.J., 1967. Mechanism of percutaneous absorption. II: transient diffusion and the relative importance of various routes of skin penetration. J. Invest. Dermatol. 48, 79–88.

Sintov, A., Krymberk, I., Daniel, D., Hannan, T., Sohn, Z., Levin, G., 2003. Radiofrequency-driven skin microchanneling as a new way for electrically assisted transdermal delivery of hydrophilic drugs. J. Control. Release 89, 311–320.

Sullivan, S.P., Murthy, N., Prausnitz, M.R., 2008. Minimally invasive protein delivery with rapidly dissolving polymer microneedles. Adv. Mater. 20, 933–938.

Sullivan, S.P., Koutsonanos, D.G., Del Pilar, D., Martin, M., Prausnitz, M.R., 2010. Dissolving polymer microneedle patches for influenza vaccination. Nat. Med. 16, 915–921.

Tokumoto, S., Higo, N., Sugibayashi, K., 2006. Effect of electroporation and pH on iontophoretic transdermal delivery of human insulin. Int. J. Pharm. 326, 13–19.

Van Damme, P., Oosterhuis-Kafeja, F., Van der Wielen, M., Almagor, Y., Sharon, O., Levin, Y., 2009. Safety and efficacy of a novel microneedle device for dose sparing intradermal influenza vaccination in healthy adults. Vaccine 27, 454–459.

Verbaan, F., Bal, S., Van den Berg, D., Groenink, W., Verpoorten, H., Luttge, R., Bouwstra, J., 2007. Assembled microneedle arrays enhance the transport of compounds varying over a large range of molecular weight across human dermatomed skin. J. Control. Release 117, 238–245.

Widera, G., Johnson, J., Kim, L., Libiran, L., Nyam, K., Daddona, P.E., Cormier, M., 2006. Effect of delivery parameters on immunization to ovalbumin following intracutaneous administration by a coated microneedle array patch system. Vaccine 24, 1653–1664.

Wilke, N., Mulcahy, A., Ye, S., Morrissey, A., 2005. Process optimization and characterization of silicon microneedles fabricated by wet etch technology. Microelectronics J. 36, 650–656.

Williams, A.C., 2003. Transdermal and Topical Drug Delivery. Pharmaceutical Press, London.